Journal of Colloid and Interface Science 441 (2015) 17–24

Contents lists available at ScienceDirect

Journal of Colloid and Interface Science

www.elsevier.com/locate/jcis

Synthesis of ultra-small cysteine-capped gold nanoparticles by pH switching of the Au(I)–cysteine polymer

Paula S. Cappellari [a], David Buceta [b], Gustavo M. Morales [a], Cesar A. Barbero [a], M. Sergio Moreno [c], Lisandro J. Giovanetti [d], José Martín Ramallo-López [d], Felix G. Requejo [d], Aldo F. Craievich [e], Gabriel A. Planes [a,*]

[a] Universidad Nacional de Río Cuarto, Ruta Nac. 36, Km 601, Río Cuarto, Córdoba, Argentina
[b] Laboratorio de Magnetismo y Nanotecnología, Instituto de Investigaciónes Tecnológicas, Universidade de Santiago de Compostela, E-15782 Santiago de Compostela, Spain[1]
[c] Centro Atómico Bariloche, Av. Bustillo 9500, 8400 San Carlos de Bariloche, Rio Negro, Argentina
[d] INIFTA, Facultad de Ciencias Exactas, Universidad Nacional de La Plata, CCT La Plata – CONICET, Diagonal 113 y 64, 1900 La Plata, Argentina
[e] Institute of Physics, University of Sao Paulo, CEP 05508-900 Sao Paulo, SP, Brazil

ARTICLE INFO

Article history:
Received 28 August 2014
Accepted 6 November 2014
Available online 15 November 2014

Keywords:
Gold nanoparticles
Cysteine
Au–cysteine polymer

ABSTRACT

We report a synthetic approach for the production of ultra-small (0.6 nm) gold nanoparticles soluble in water with a precise control of the nanoparticle size. Our synthetic approach utilizes a pH-depending Au–cysteine polymer as a quencher for the AuNPs grown. The method extends the synthetic capabilities of nanoparticles with sizes down to 1 nm. In addition to the strict pH control, the existence of free –SH groups present in the mixture of reaction has been observed as a key requirement for the synthesis of small nanoparticles in mild conditions. UV–Vis, SAXS, XANES, EXAFS and HR-TEM, has been used to determinate the particle size, characterization of the gold precursor and gold–cysteine interaction.

1. Introduction

Metal nanoparticles (NP) have been subject of intense investigation in the last twenty years, mainly due to fundamental and applied aspects relevant to the quantum size effects [1,2]. As a result of the high fraction of atoms on NP surface the resulting physical properties of small NP there are neither those of bulk metal, nor those of molecular compounds. In general the physical properties depend on the particle size, shape, capping agent and host [3]. For example, small ($d \sim 1$ nm) gold nanoparticles (AuNPs) show properties such as fluorescence [4] and redox-type charge behavior [5,6]. For such small particle size, no significant differences in the UV–Vis region has been observed when compared with the absorption of noncovalent Au(I)–Au(I) interacting complexes in nearby packed polymer structures containing gold (I); see for example the results by Briñas et al. [7] and those by Negishi et al. [8] In particular, Negishi et al. have proposed that the thiolated subnanometer-sized Au clusters constitute a different type of binary system which lies between the Au(I)–thiolate complexes and thiolate-protected Au NP [8].

While a great number of synthetic routes are suitable for production of Au NP with size in the tens nanometer scale, there are only a few methods to synthesize Au NP with size below 1.5 nm in a controlled manner [9]. One of the most used approaches utilize the fragmentation of bigger AuNPs into ultra-small particles (denoting as USP, NP with size below 1.5 nm), induced by the excess of –SH group in the capping agent, frequently small biomolecules via a thiolate linkage to Au [10,11]. Sarangi et al. [12] reported fluorescent properties of Au NP capped with cysteine (Cys) obtained by direct chemical reduction in presence of the amonoacid. However, the lack of information about the synthetic procedure (for example, pH and purification of the samples) makes it difficult to discriminate the contribution from the also fluorescent Au(I)–Cys complex to the observed signal. By using a similar method to the one proposed in this work, Brinas et al. [7] developed a method for preparing size-controllable Au NP capped with glutathione by varying the pH before reduction. They proposed a mechanism based on the formation of polymeric nanoparticle precursor, Au(I) glutathione polymers, which changes size and density depending on the pH (a pH-responsive coordination polymer). The authors report the synthesis of gold nanoparticles with size between 2 and 6 nm. Indeed, in the last years had been made notorious advances in the understanding of the chemistry of such coordination polymers [13–15]. The success of such polymers, formed by non-covalent interactions, lie in the possibility of perform

* Corresponding authors. Fax: +54 358 4676233.
E-mail address: gplanes@exa.unrc.edu.ar (G.A. Planes), gplanes@exa.unrc.edu.ar (G.A. Planes).
[1] On leave from.

http://dx.doi.org/10.1016/j.jcis.2014.11.016
0021-9797/

a mechanical/chemical response as result of a external triggering (stimuli), which lead its central application as smart materials and sensors [16].

In this work, we use Au(I)–cysteine as precursor. Due to the zwitterionic nature of the aminoacid, the coordination polymer composed of –[Au(I)-Cys]$_n$– units is pH responsive. The strategies for AuNP synthesis and size control is based in the chemical reactivity during the polymer switching between two very stables –[Au-SH)]$_n$– states. A strong dependence of the reaction kinetics and pH switching on the existence of additional –SH groups was also observed. X-ray Absorption Near Edge Structure (XANES) and Extended X-ray Absorption Fine Structure (EXAFS) Spectroscopy were used for *in-situ* characterization of the AuCys complex; while a combination of Small-Angle X-ray Scattering (SAXS) and HR-TEM were used for the evaluation of the NP size.

2. Materials and methods

2.1. Chemicals

L-*cysteine* 98% (Lancaster), $NaBH_4$ 95% (Carlo Erba), NaOH 99% (Merck) and HCl 37% Fisher Scientific, were used as received. All aqueous solutions were prepared with Type I water (18 MΩ-cm, ELGA, Purelab Classic) (DI water).

2.2. Dissolutions

100 ml of solution 0.01 M of cysteine in acid media (ACys) was prepared by mixing 0.12 g of cysteine, 5 ml of HCl 0.5 M and completed until 100 ml with DI water. The acid Au–cysteine precursor (AAuCys) was prepared a few minutes before each synthesis by addition of 0.5 ml of 50 mM $HAuCl_4$ to 24.5 ml of the ACys solution, to give pH = 2.5. Cysteine in basic media (BCys) was prepared by mixing 0.12 g of cysteine, 5 ml of NaOH 0.5 M and completed until 100 ml with DI water. The analogous basic Au–cysteine precursor (BAuCys), was obtained by mixing of 0.5 ml of 50 mM $HAuCl_4$ and 24.5 ml of the BCys solution, to give pH = 10.5. The $NaBH_4$ solution in water (0.01 M) was prepared a few minutes before use and preserved in an ice bath until the moment of use.

2.2.1. Synthesis of Au nanoparticles

AuNPs were synthesized following two opposite routes, giving similar results. In the first the AuNPs are obtained increasing the pH value of the precursor in presence of $NaBH_4$, denoted as *Route a*; and the second by fast pH decreasing, denoted as *Route b*. All chemical reactions were performed at 25 °C, and more details are given below:

Route a: Starting from the AAuCys solution (pH = 2.5) in presence of $NaBH_4$ (0.01 M), followed by fast addition (vortex mixing) of a given volume of NaOH 0.1 M. The final pH of the reaction media depends on the added volume of NaOH, and may be adjusted between 4 and 11.

Route b: Starting from the BAuCys solution (pH = 10.5) in presence of $NaBH_4$ (0.01 M), followed by fast addition (vortex mixing) of a given volume of HCl 0.1 M. The final pH of the reaction media depends on the added volume of HCl, and may be adjusted between 9 and 2.

2.2.2. HRTEM

High-resolution transmission electron microscopy (TEM) images were obtained using a Philips CM200 UT transmission electron microscope operated at 200 kV and room temperature. Although the samples are stable over periods longer than one day, we study them immediately to their synthesis. We minimize the supplied dose to the sample by spreading the electron beam.

2.2.3. SAXS, XANES and EXAFS experiments

SAXS measurements were performed using the SAXS-1 beam line of the National Synchrotron Light Laboratory (LNLS), Campinas, Brazil [17]. The SAXS intensity curves were determined using a 2D Pilatus detector as functions of the modulus of the scattering vector $q = 4\pi\sin\theta/\lambda$, θ being half the scattering angle and λ the X-ray wavelength, $\lambda = 1.61$ Å. The SAXS curves were normalized to the intensity of the direct X-ray beam to compensate for the continuous decrease in emission of the synchrotron source. Since the incident X-ray beam has a point-like cross-section no corrections of the experimental SAXS curves for smearing effects were needed.

The liquid samples to be studied were placed inside a cell with two thin and parallel mica windows for transmission SAXS measurements. A cell, with a specially designed geometry allowed the simultaneous filling with the three precursor reactives, and further in situ follow-up of the reaction. In order to study the effects of pH on the size features of the Au NPs, the pH was varied, starting from pH = 10.5 down to different stepped final values.

XANES and EXAFS experiments were carried out at the XAFS2 beamline at the LNLS. EXAFS spectra at the Au L_3 (11,919 eV) edge were recorded at room temperature using a Si (1 1 1) single channel-cut crystal monochromator in transmission mode and with three ion chambers as detectors. The third one was used to measure the corresponding metallic reference simultaneously with the sample. Samples were sealed in special sample holders with kapton windows for liquids.

XANES spectra were normalized and energy aligned using the Au foil spectrum measured simultaneously with each sample. The EXAFS data were extracted from the measured absorption spectra by standard methods using the ATHENA software which is part of the IFFEFIT package [18]. The Fourier transformation was calculated using the Hanning filtering function. EXAFS modeling was carried out using the ARTEMIS program (IFFEFIT package) [11]. Structural parameters (coordination numbers and bond lengths and their mean squared disorders) were obtained by a non-linear least-squares fit of the theoretical EXAFS signal to the data in R space by Fourier transforming both the theory and the data. Theoretical scattering path amplitudes and phase shifts for all paths used in the fits were calculated using the FEFF6 code [19]. The *k*-range was set from 2 to 12 Å^{-1} and the Fourier transform were fitted in the R-range: 1.2–2.3 Å. The passive reduction factor S_0^2 was set to a value of 0.93. This value was obtained from fitting metallic Au foil standard by constraining the coordination number in this compound of known crystal structure.

3. Results

3.1. Stability of the Au(I)–Cys precursor in presence of $NaBH_4$

The spontaneous formation of the precursor Au(I)-Cys in acid media (AAuCys), prepared by mixing cysteine and Au(III) compound, has been reported previously [8]. In this process, Au(III) is reduced by the thiol group present in the structure of cysteine, to give an opalescent dispersion of the –[Au(I)-Cys]$_n$– polymer. It is interesting to note that a similar precursor is obtained at pH = 10.5. In fact, a decrease of the pH from 10.5 to 2.5 results in the spontaneous emergence of opalescence, characteristic of the polymer –[Au(I)-Cys]$_n$– at this pH, as reported in Ref. [8]. At pH < 5, appears a peak at 365 nm originate by the metal centered charge transfer in the –[Au(I)-Cys]$_n$– polymer due to Au(I)–Au(I) interaction (Fig. 1 SI) [7,20]. In some cases, if the final pH after reduction is situated below 5, this peak positioned at 365 nm

remain visible after reduction, due to the existence of some residual –[Au(I)-Cys]$_n$– polymer.

The addition of 0.5 ml of $NaBH_4$ 0.01 M to 4 ml of the AAuCys do not produce any significant changes in the appearance – white and opalescent due to the polymer – on the time scale of hours. This observation indicates that even a strong reducing agent, such as BH_4^-, cannot reduce the precursor to give AuNPs. In fact, the resulting solution remains unaltered in the time, as show the absence of any change in the UV–Vis. In a similar manner, when 0.5 ml of $NaBH_4$ 0.01 M is added to 4 ml of the BAuCys, the solution,clear and colorless, remain unaffected, with the absence of any visible absorption band assignable to the surface plasmon resonance of Au NPs (i.e. see black line in Fig. 4 SI). The SAXS analysis of both samples only detects polymer agglomeration, in good agreement with previous measurements by Dynamic Light Scattering (DLS, not shown) [7]. Control reactions of $NaBH_4$ with Au(III) solution in absence of cysteine were realized in order to corroborate the reduction capability of $NaBH_4$ at pH 2.5 and 10.5 respectively. After the addition of $NaBH_4$ to the solution containing Au(III), the color of the reaction mixture change immediately to the characteristic ruby-red of Au NPs.

3.2. Synthesis of small cysteine-capped gold nanoparticles

As is described in the experimental part, a straightforward synthesis of ultrasmall AuNPs (~1 nm) is possible by just adding to the previous protocol a second step; the subsequent change of pH at the reaction solution. For simplicity, the method described here for AuNPs synthesis and the corresponding results are illustrated only for the procedure denoted as *Route a*. As was explained above, the first step consists in the addition of 0.5 ml of $NaBH_4$ 0.01 M to 4 ml of the AAuCys solution, under vigorous stirring. Then, in a second step, an aliquot of 0.5 ml of NaOH 0.1 M is added, changing suddenly the pH from ~2.5 to ~11. The modification of the pH produces an instantaneous variation in the color of the solution, from clear white to light yellow (see the UV–Vis spectra in Fig. 1, black line). If, alternatively, the procedure is carried out changing the volume of the aliquots of NaBH4 0.01 M (to give a final pH of the reaction mixture en the range between 4 and 11) the coloration observed is different for each case.

Those results, summarized for four different final value of pH, are shown in Fig. 1 (UV–Vis) and Fig. 2 (HRTEM,). The UV–Vis spectra corresponding to AuNP synthesized at a final pH near 11 (Fig. 1, black line) shows a strong absorption band, with onset at 800 nm, associated in literature to small gold clusters [10], and the absence of the band near 520, frequently associated to Au NP plasmon [21,22]. In fact, the absorption extends in the region between 280 and 700 nm with a shoulder at ~380 nm. The corresponding HRTEM images (Fig. 2(A)) shows the presence of small AuNP with an average diameter around 1.2 nm. Fig. 2A also shows several AuNP with sizes that largely exceed the 1.2 nm. The presence of larger AuNP in dissolution should produce a noticeable red shift in the absorption spectrum, however this is not observed in the samples tested. On the other hand, a visible growth of AuNP was observed after few minutes of exposition to the electron beam during the TEM experiments. Based on the above stated observations, we suggest the ex-situ conditions as the principal cause of the size enlargement. This process probably involves the presence of unreacted precursor Au(I)–Cys complex surrounding the AuNP which is reduced during HRTEM analysis [23].

Using the same strategy, but decreasing the amount of NaOH added during the last step, the final pH can be adjusted to 9.5. Under these conditions, the presence of the plasmon absorption at 550 nm starts to become visible (red line, Fig. 1). It must be noted that all the features observed in the UV–Vis spectrum have been associated in the literature to AuNPs with diameters below 2 nm [10,21,24–26]. The HRTEM image (Fig. 2B) shows AuNP with a size close to 3 nm. Studies for other intermediate values of final pH are summarized in Fig. 1. The absorption peak at 380 nm is clearly defined when the final pH for the synthesis is close to 7.3 (green line, Fig. 1) while the peak at 530 nm is only visible for a final pH of around 6 (blue line, Fig. 1).

From a direct interpretation of the HRTEM and UV–Vis, it could be deduced that bigger (5–7 nm) AuNP were synthesized when the final pH was adjusted in the range of 6–8. While the observed trend in the nanoparticle size is correct, as will be show below in the text, the sizes obtained by HRTEM should be checked by in-situ techniques, like SAXS. The reason was stated above: the existence of nanoparticles growing in the TEM column. On the other hand, the cysteine adsorbed on gold nanoparticles can donate an electron pair into unoccupied orbitals of gold on the particle surface. In this way, the particles receive a negative charge density (δ^-) which may induce a red shift in surface plasmon peak [10].

Similar results are obtained for the procedure denoted as *Route b*, starting with BAuCys, then adding $NaBH_4$ 0.01 M and finally, HCl 0.1 M, changing the pH from the original value of 10.5 to different final pH values (between 9 and 2).

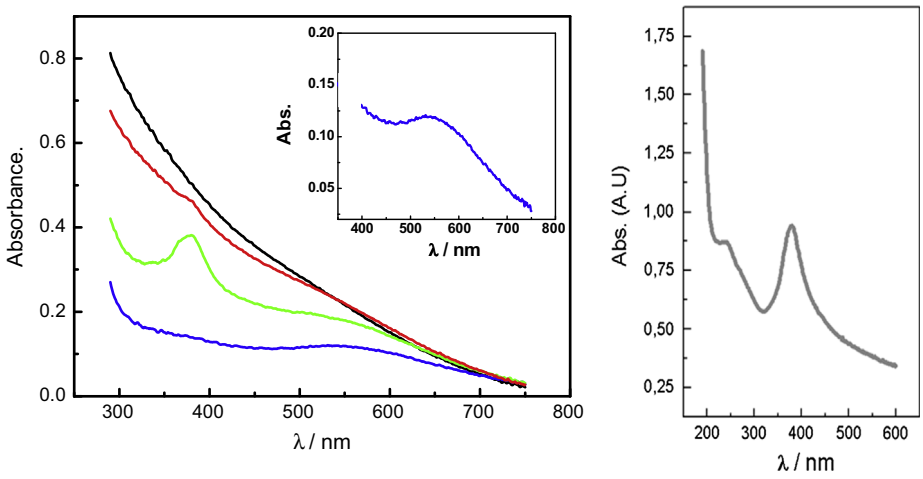

Fig. 1. Left. UV–visible spectra of AuNPs in the reaction solutions, obtained following the route (a). Final pH = 11 (black line), pH = 9.5 (red line), pH = 7.3 (green line), pH = 6 (blue line). Inset; Rescaling of the UV–Visible spectra at pH = 6, showing the plasmon with more detail. Right UV–visible spectra of AuNPs in the reaction solutions obtained following route (b), final pH = 3. (For interpretation of the references to color in this figure legend, the reader is referred to the web version of this article.)

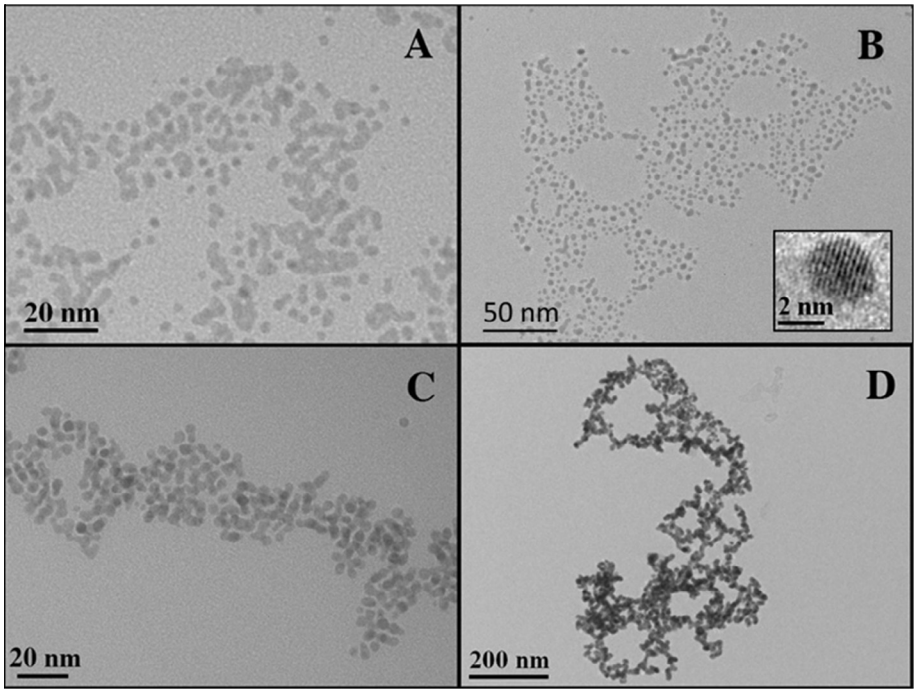

Fig. 2. HR-TEM image of cysteine-capped AuNPs. These AuNPs were obtained by pH jumping from an initial pH = 2.5, to different final pH: (A) pH = 11; (B) pH = 9.5; (C) pH = 7.3; (D) pH = 6.

3.3. Size determination by SAXS

Due to the difficulties in size determination for the smallest AuNPs, we decide to perform SAXS experiments. Due to experimental limitation, the SAXS analysis was performed following the procedure denoted as (b). The SAXS curves displayed in Fig. 3a correspond to colloidal liquid solutions containing Au NPs in their final stage of development – i.e., when the evolution of the sizes of the nanoparticles has stopped – with their final pH values set equal to 3, 8 and 9. The UV–Vis of the AuNPs obtained with final pH = 3 is shown in the right side of Fig. 1.

In order to determine the NP sizes we have analyzed the SAXS curves starting from a simple model of a dilute solution containing a monodisperse set of spherical NPs. This approach is well justified by the HRTEM results, showing that isolated nanoparticles are quite spherical. The experimental SAXS curves plotted in Fig. 3a do not exhibit the classical shapes that are expected for a set of identical spherical NPs, i.e. $I(q) \propto v^2|\Phi(q,R)|^2$, where v is the NP volume and $\Phi(q,R)$ is the theoretical form factor associated to the scattering amplitude of spherical NPs, $\Phi = 3[\sin(qR) - qR\cdot\cos qR)]/(qR)^3$ [27]. The second step was to assume a distribution of NP radii, $N(R)$, described by the lognormal function. The SAXS intensity function $I(q)$ that was applied for the modeling of the experimental SAXS curves is given by

$$I(q) \propto \int N(R)R^6\Phi(q,R)dR \quad \text{where} \quad N(R) = \frac{1}{R\sigma\sqrt{2\pi}}e^{-\frac{(\ln R-\mu)^2}{2\sigma^2}} \qquad (1)$$

The size distribution $N(R)$ associated to the modeled $I(q)$ function that exhibits a good fitting to the experimental SAXS curve corresponding to the samples with final pH equal to 3, 8 and 9

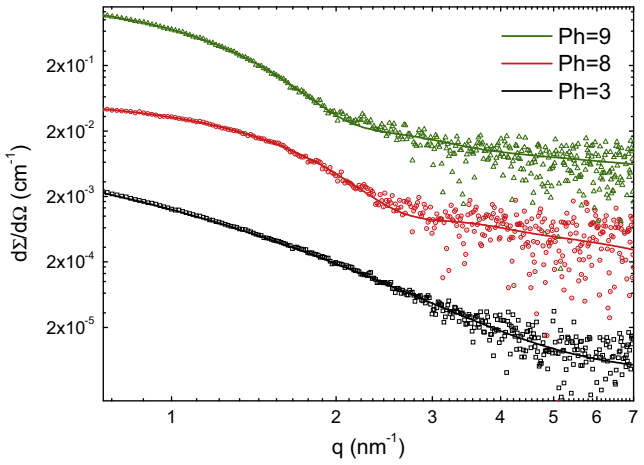

Fig. 3a. Symbols: Experimental SAXS intensity curves corresponding to samples with final pH equal to 3, 8 and 9. Solid lines: Modeled intensity curves that best fit to the experimental SAXS curves. Curves are vertically displaced.

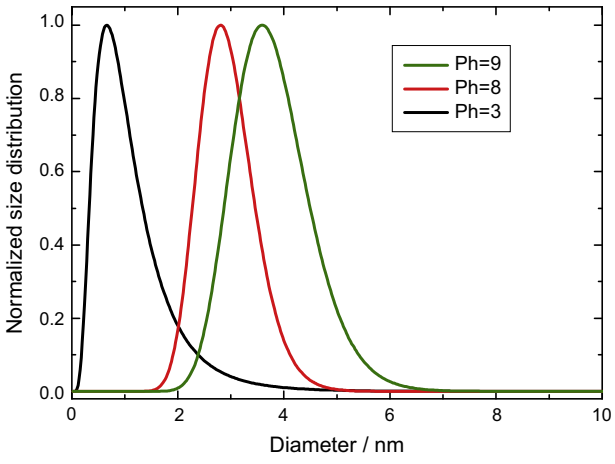

Fig. 3b. Normalized size distribution functions derived from the analysis of the SAXS curves plotted in Fig. 1.

(Fig. 3a) are plotted in Fig. 3b. The main size parameters derived from the described analyses of our SAXS results are reported in Table 1.

3.4. XANES and EXAFS analysis

The surprisingly high stability of the precursor demand further analysis to identify the chemical nature in the immediate vicinity of the gold atom, and its oxidation state. With this purpose, XANES and EXAFS spectroscopy were used. The in-situ characterization of the oxidation state of gold in [AuCys] precursor at two pH values was carried out by means of XANES spectroscopy at the Au L_3 edge and results are shown in Fig. 4. The L_3 absorption edge of transition metals exhibits important features which can probe the occupancy of *d*-states. For instance, third-row transition metals exhibit a large peak after the absorption edge, usually called "white line", which primarily corresponds to the electric dipole allowed electronic transition from 2*p* states to 5*d* ones. The white line intensity is directly related to the density of unoccupied states.

Little [28] studied the L_3 absorption edge of Au, Pt, Ir and Ta and showed that the "white line" increased as the number of 5*d* holes increases. This gave an instrument to estimate the density of empty states in third period transition metals. Mansour et al. [29] and Ankudinov et al. [30] proposed methods for the determination of the number of empty states through measuring L_2 and L_3 absorption edges. In particular, the Au L_3-edge XANES spectrum of metallic Au does no present a white line as the *5d* states are almost full. In addition, it has been shown that, for the third row transition metals, the position of the absorption edge and the intensity of the white line at the L_3 edge are both directly related to the oxidation number of the absorbing atom [31]. The higher the oxidation state of the metal, the more positive the overall charge of the atom and more energy is required to excite an electron out of an orbital [32,33]. As the oxidation number of the absorbing atom increases, the edge moves to higher energy and the intensity of the white line increases because of the higher density of empty states. For both energy shifting and white line intensity variations, XANES becomes an ideal tool for the determination of changes in the oxidation state of metals.

The change in the oxidation state of Au is observed for both Au–cysteine complexes in acid and basic solutions with respect of the metallic gold (Fig. 4). The position of the edge moves to higher energy and there is an increase of the "white line" intensity for the Au–cysteine complexes. The trend is that in acid solution the edge shifts to higher energy than in basic solution and the increase in the white line is bigger. Both are indications that gold is more reduced in basic solution.

Fig. 5 shows the EXAFS spectra and their corresponding Fourier transforms of Au–cysteine complexes. EXAFS spectroscopy gives structural information of the surroundings of the absorbing atom. In particular, the type, number and bond distance of the atoms in the first shells can be determined. Both present a peak at 1.8 Å without phase corrections indicating the presence of light neighbors in the first shell coordination. No evidence of gold atoms is observed as almost no peak is present in the 2–3 Å regions. In order to quantitatively analyze this data, the main peaks were isolated and fitted using standard procedures. Different light atoms were used to fit both spectra: N, O and S. Fitted functions are shown as solid lines in the Fourier transforms of Fig. 5. The obtained results are shown in Table 2. Nitrogen and Oxygen atoms could not fit well the data and only a shell of sulfur atoms resulted in a good fit with well behaved parameters. In both cases 2 sulfur atoms are found in the first shell of Au atoms. However a slight difference in the Au–S distance was found: 2.31 Å for the basic solution and 2.28 Å for the acid one. This shorter bond distance for the acid solution is an indication of a higher oxidation state in accordance with XANES results [34]. In addition, there is a big increase in the Debye–Waller factor in the acid solution probably meaning that in that case the Au–cysteine complex is more disordered and less well defined.

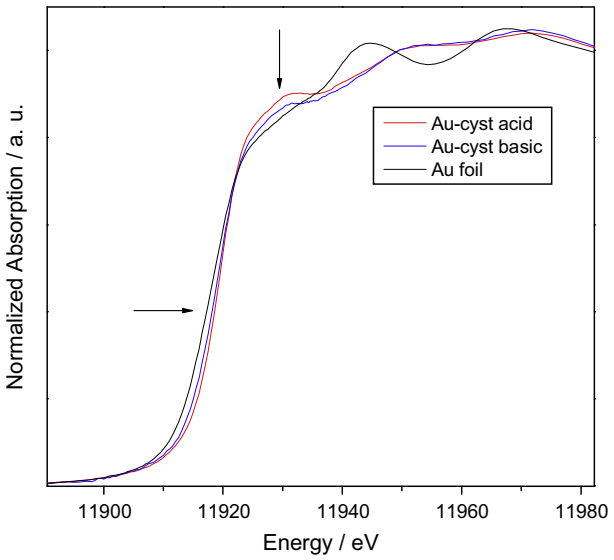

Fig. 4. XANES spectra at the Au L_3 edge of Au–cysteine complexes in acid (red line) and basic (blue line) solutions compared with that of metallic gold (black line). (For interpretation of the references to color in this figure legend, the reader is referred to the web version of this article.)

Considering the results obtained by XANES and EXAFS for the reaction precursors, we can conclude that pH does not only modify the charge state of the polymer, as stated before for Au-SGH polymers [7], but it also modifies the oxidation state of the metallic centers.

4. Discussion

Briñas et al. have studied a similar method to synthesize AuNP using glutathione (SGH) as capping agent instead of cysteine [7]. The authors report a method to synthesize size-controllable gold nanoparticles with diameters ranging from 2 to 6 nm capped with glutathione by varying the pH of the solution before reduction. The size controllability has been attributed to the dependence of the size of the AuNP precursor, –Au(I)–Gluthatione–, with the pH. The observed diameter of the AuNP became smaller when the pH apart from the isoelectric point (IP) of the GSH (near pH 3). In the particular case of Cys, with an IP close to 5, we test the reaction at pH below and over the IP. The dependence of size with pH observed in our study is in agreement with the mechanism proposed by Briñas et al. [7].

However, it should be noted that the strategy for the synthesis of smaller nanoparticles, (around 1 nm) and size control explored here is quite different to that reported by Briñas et al. [7], where the pH is adjusted before reduction. In fact, we fail trying to extend

Table 1
Parameters obtained from the fitting procedure of SAXS curves. We report the number of nanoparticles per unit volume N_p (in arbitrary units), the arithmetic radius average, $\langle R\rangle = e^{\mu+\frac{1}{2}\sigma^2}$, and its standard deviation $sd = ((e^{\sigma^2}-1)\langle R\rangle^2)^{1/2}$ for each sample with different pH values.

	pH 9	pH 8	pH 3
N_p (arb. units)	7.94 ± 0.07	9.7 ± 2	390 ± 10
$\langle R\rangle$ (nm)	1.862 ± 0.006	1.490 ± 0.009	0.6 ± 0.1
sd (nm)	0.191 ± 0.002	0.166 ± 0.003	0.37 ± 0.08

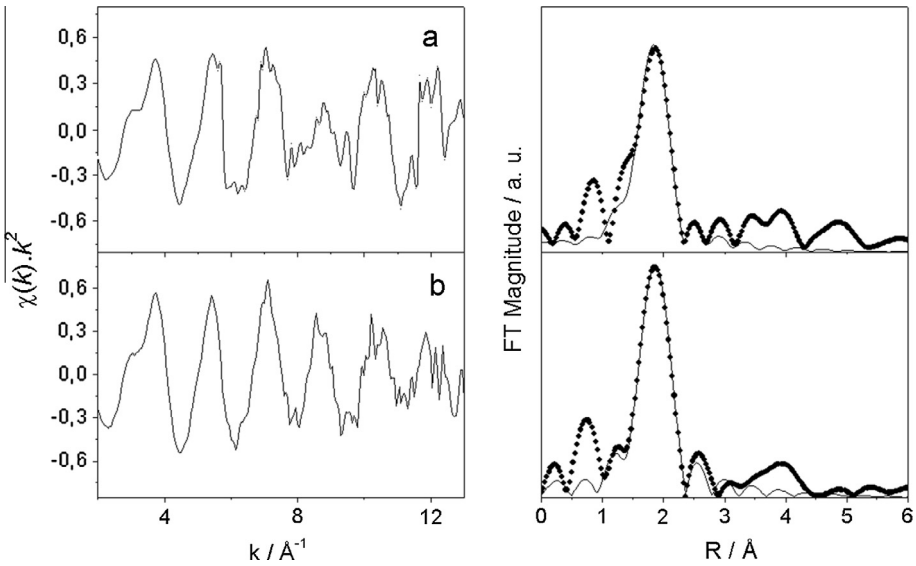

Fig. 5. EXAFS spectra of Au–cysteine complex in (a) acid and (b) basic solution (right) and their corresponding Fourier transforms (circles, left) and the fitted functions (solid lines, left).

Table 2
Results obtained from the fittings shown in Fig. 5.

	N	R (Å)	σ^2 (Å^{-2})	E_0 (eV)
Au-cys Basic	2.0 ± 0.2	2.31 ± 0.01	0.003 ± 0.001	4 ± 1
Au-cys Acid	2.2 ± 0.5	2.28 ± 0.02	0.007 ± 0.002	3 ± 1

N: Average coordination number, R: Interatomic distance, σ^2: Debye–Waller factor, E_0: Energy shift parameter.

the published method [7], to the synthesis of ultrasmall gold nanoparticles, because in these conditions, the low reactivity requires excessive concentrations of $NaBH_4$, leading to side reactions. However, the same inhibition of the complex reactivity at 3 > pH > 9 provides the key to solve the problem, and was used here for quenching the NP growth. The null reactivity of the complex at 3 > pH > 9, where the synthesis of smaller gold nanoparticles is expected, makes necessary the addition of a further step, the pH change. This essential variation extends the synthesis capabilities to sizes below 1 nm without further increasing of $NaBH_4$ concentration. However, as a consequence of this fast quenching, an indeterminate fraction of the Au cations stay unreduced in the reaction media, which explain the different number of particles obtained in each experiment and the further particle grown in the TEM column.

4.1. Effect of free –SH group on reactivity

Additional experiments in absence of free –SH groups were performed. In fact, after removal of the excess of Cys by centrifugation, the process of switching between the acid and basic form of the precursor is not possible or is very slow (Fig. 2 SI). Obviously, the size control under this condition is also impossible. Additionally, a strong dependence of the reaction velocity with the concentration of Cys present in the mixture of reaction was observed. This experiment reveals an interesting detail of the reaction mechanism. The addition of any soluble compound containing –SH group (i.e. 2-aminoethanethiol) revert this situation and the system recover the reversibility between the acid and basic form (Fig. 3 SI).

An explanation for this fact could be that the rearrangement of the polymeric precursor, as a consequence of the change of the pH, requires of "mobile" free –SH groups as circumstantial replacement of the "rigid" –SH groups which form part of the polymeric chain –[Au-SH)]$_n$–. Even more, has been observed that this lack of mobility also obstruct the Au(I) reduction, pointing to the polymer reordering as one of the possible causes of Au exposure to reducing agent. However, since there are other groups capable of interacting with the Au(I), it is unclear whether the change in pH is also accompanied by a change in the chemical nature of the complex, metal oxidation state, etc. At this point, the XANES and EXAFS analysis provides evidence that some additional interactions between the metal centers and the cysteine molecules are also present in this condition. In acid solution the edge shifts to higher energy than in basic solution and the increase in the white line is bigger. Both are indications that gold is more reduced in basic solution; this fact is consistent with the acid characteristic of the thiol. Additionally, EXAFS also provide solid evidence that is the S atom, and not other, the linker between Au(I) and cysteine at any pH. This fact reduce the possibilities, pointing to the –[Au-SH)]$_n$– reordering as the main cause of reactivity.

The results of the SAXS measurements confirm the previous observations by TEM regarding the formation of ultrasmall Au NPs when the pH is changed between both nonreactive states (Note that in this case, the AuNPs were obtained by pH jumping from an initial pH = 11 to pH = 3, pH = 8 and pH = 9 respectively). The clearly different features of the curves displayed in Fig. 3b indicate that the size of the Au NPs strongly depends on the final pH value. All samples exhibit a single mode volume weighted radius distribution, with a higher average diameter as the pH is increased.

Finally, the inhibitory role played by the cysteine, hindering the Au+ reduction at pH < 3 and pH > 9 (see scheme 1) is clear. The dependence of the reaction kinetics on the existence of additional –SH groups observed here, suggests that some additional requisite must be satisfied in this last case to make reduction feasible, as the existence of "free" –SH groups, what affects the rate of polymer reordering and is a necessary requirement during the Au(I) to Au(0) reduction. This assumption is also supported by the observed slow (or absent) complex inter-conversion when pH is changed in the absence of others –SH groups. *Per-se*, those –SH group bonded to Au(I) have reduced "mobility", as it occurs in intercrossed polymers, where any conformational change is energy penalized.

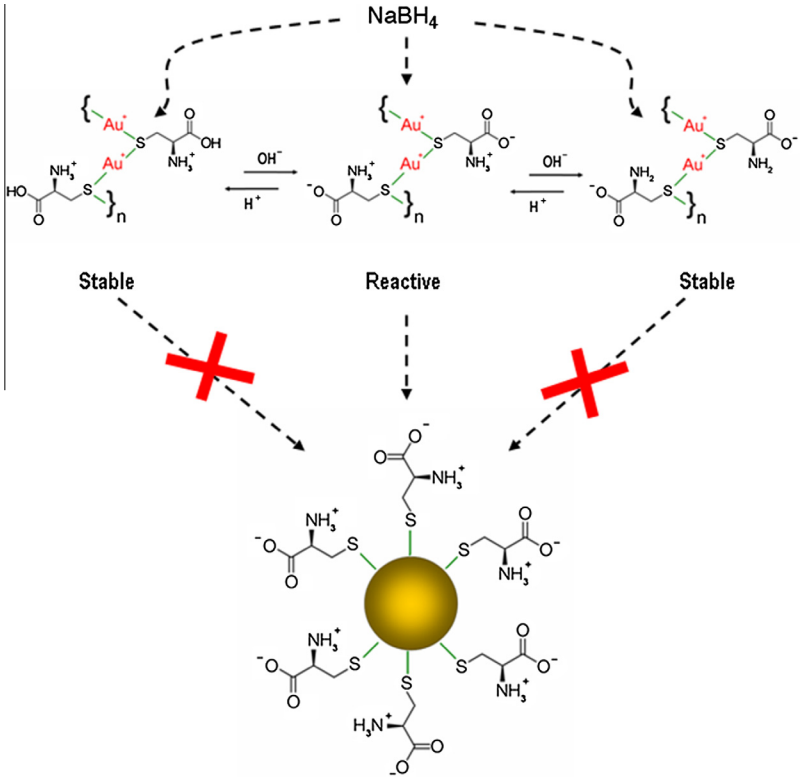

Scheme 1. Correlation between structure, reactivity and pH of the AuCys complex.

5. Conclusion

We report a synthetic approach for the production of ultrasmall (0.6 nm) gold nanoparticles soluble in water with an accurate size control. The strategies for AuNP synthesis and size control is based in the chemical reactivity of a transition state between two very stables $-[Au\text{-}SH)]_n-$ states. The extension to extreme pH condition and the use of pH jump let us synthesize ultras-mall, stable gold nanoparticles. Due to the zwitterionic nature of the aminoacid, the structure of the Cys–Au polymer is strongly depending on pH. So, if pH is changed from one of the stable states to the other, a reactive (transition) state is achieved for a short period of time during the polymer reordering. The fact that Au cations are exposed to $NaBH_4$ in this stage is easily evidenced by the formation of small yellow–brown AuNP. The permanence in that reactive state ($4 < pH < 9$) lets to the ultrasmall AuNPs to grow, being the final size controlled by the pH.

This fact implies that the polymer should be necessarily rearranged after any pH change. The main consequence of such alteration on polymer structure is the fast exposure of the Au(I) to the reductant and the consequent reduction from Au(I) to Au(0).

Finally, the combined use of SAXS, XANES, EXAFS and HRTEM allows a better understanding of this unusual reaction mechanism.

Acknowledgments

The authors thank financial support from Agencia Nacional de Promoción Científica y Tecnológica (Argentina, Project PICT 2010-2421), CONICET (Argentina, Project PIP 112-201101-01035), UNLP, Laboratorio Nacional de Luz Sincrotron (LNLS, Campinas – Brazil, projects SAXS1-9346 SAXS1-9960 and XAFS1-11695). GMM, CAB, MSM, FGR, LJG, JMRL and GAP are permanent research fellows of CONICET. PSC thank to CONICET for a graduate fellowship.

Appendix A. Supplementary data

Supplementary data associated with this article can be found, in the online version, at http://dx.doi.org/10.1016/j.jcis.2014.11.016.

References

[1] M-C. Daniel, D. Astruc, Chem. Rev. 104 (1) (2004) 293–346.
[2] Oxana V. Kharissova, Boris I. Kharisov, V.B. Jiménez-Pérez, B. Muñoz Flores, U. Ortiz Méndez, RSC Adv. (3) (2013) 22648–22682.
[3] Kenneth J. Klabunde (Ed.), Nanoscale Materials in Chemistry, Copyright 2001 John Wiley & Sons, Inc., ISBNs: 0-471-38395-3.
[4] H. Duan, S. Nie, J. Am. Chem. Soc. 129 (9) (2007) 2412–2413.
[5] H. Zhang, G. Schmid, U. Hartmann, Nano Lett. 3 (3) (2003) 305–307.
[6] B.M. Quinn, P. Liljeroth, V. Ruiz, T. Laaksonen, K. Kontturi, J. Am. Chem. Soc. 125 (22) (2003) 6644–6645.
[7] R.P. Briñas, M. Hu, L. Qian, E.S. Lymar, J.F. Hainfeld, J. Am. Chem. Soc. 130 (3) (2008) 975–982.
[8] Y. Negishi, Y. Takasugi, S. Sato, H. Yao, K. Kimura, T. Tsukuda, J. Phys. Chem. B 110 (25) (2006) 12218–12221.
[9] C. Gautier, T. Bürgi, J. Am. Chem. Soc. 128 (34) (2006) 11079–11087.
[10] Tie Wang, Xiaoge Hua, Shaojun Dong, Chem. Commun. (2008) 4625–4627.
[11] C-Y. Ke, T-H. Chen, L-C. Lu, W-L. Tseng, RSC Adv. 4 (2014) 26050–26056.
[12] S.N. Sarangi, A.M.P. Hussain, S.N. Sahu, Appl. Phys. Lett. 95 (2009) 073109/1–073109/3.
[13] C. Liu, G. Li, G. Pang, R. Jin, RSC Adv. 3 (2013) 9778–9784.
[14] J.-S. Shen, D-H. Li, M-B.K. Zhang, J. Zhou, H. Zhang, Y-B. Jiang, Langmuir 27 (1) (2011) 481–486.
[15] C. Yu, L. Zhu, R. Zhang, X. Wang, C. Guo, P. Sun, G. Xue, J. Phys. Chem. C 118 (2014) 10434–10440.
[16] W. Li, Y. Kim, J.J. Li, M. Lee, Soft Matter 10 (2014) 5231–5242.
[17] G. Kellerman, F. Vicentin, E. Tamura, M. Rocha, H. Tolentino, A. Barbosa, A. Craievich, I. Torriani, J. Appl. Crystallogr. 30 (1997) 880–883.
[18] B. Ravel, M. Newville, J. Synchrotron Radiat. 12 (2005) 537–541.
[19] S.I. Zabinsky, J.J. Rehr, A. Ankudinov, R.C. Albers, M.J. Eller, Phys. Rev. B 52 (4) (1995) 2995–3009.
[20] H. Nie, M. Li, Y. Hao, X. Wanga, S. Xiao-An Zhang, Chem. Sci. 4 (2013) 1852–1857.
[21] W.W. Weare, S.M. Reed, M.G. Warner, J.E. Hutchison, J. Am. Chem. Soc. 122 (2000) 12890–12891.
[22] T.K. Sham, P-S.G. Kim, P. Zhang, Solid State Commun. 138 (2006) 553–557.

[23] G. Corthey, L.J. Giovanetti, J.M. Ramallo-López, E. Zelaya, A.A. Rubert, G.A. Benitez, F.G. Requejo, M.H. Fonticelli, R.C. Salvarezza, ACS Nano 4 (6) (2010) 3413–3421.
[24] M.M. Alvarez, J.T. Khoury, T.G. Schaaff, M.N. Shafigullin, I. Vezmar, R.L. Whetten, J. Phys. Chem. B 101 (1997) 3706–3712.
[25] Y. Negishi, K. Nobusada, T. Tsukuda, J. Am. Chem. Soc. 127 (2005) 5261–5270.
[26] J. Zheng, J.T. Petty, R.M. Dickson, J. Am. Chem. Soc. 125 (2003) 7780–7781.
[27] O. Kratky, O. Glatter, Small-Angle X-ray Scattering, Academic Press, London, 1982.
[28] F. Lytle, J. Catal. 43 (1976) 376–379.
[29] A.N. Mansour, J.W. Cook Jr, D.E. Sayers, J. Phys. Chem. 88 (1984) 2330–2334.
[30] A.L. Ankudinov, A.I. Nesvizhskii, J.J. Rehr, J. Synchrotron Rad. 8 (2001) 92–97.
[31] T. Pauporté, D. Aberdam, J.L. Hazemann, R. Faure, R. Durand, J. Electroanal. Chem. 465 (1) (1999) 88–95.
[32] R.G. Shulman, Y. Yafet, P. Eisenberger, W.E. Blumberg, Proc. Natl. Acad. Sci. U.S.A. 73 (1976) 1384–1388.
[33] J.M. Ramallo-López, E.J. Lede, F.G. Requejo, J.A. Rodriguez, J-Y. Kim, R. Rosas-Salas, J.M. Domínguez, J. Phys. Chem. B 108 (2004) 20005–20010.
[34] I.D. Brown, D. Altermatt, Acta Crystallogr. B41 (1985) 244–247.